Preparation, Crystallization, and Properties of Biodegradable Poly(butylene adipate-*co*-terephthalate)/ Organomodified Montmorillonite Nanocomposites

Fang Yang, Zhaobin Qiu

State Key Laboratory of Chemical Resource Engineering, Beijing University of Chemical Technology, Beijing 100029, China

Received 13 January 2010; accepted 12 April 2010
DOI 10.1002/app.32619
Published online 18 August 2010 in Wiley Online Library (wileyonlinelibrary.com).

ABSTRACT: Intercalated and exfoliated nanocomposites of biodegradable poly(butylene adipate-*co*-terephthalate) (PBAT) and Cloisite 30B (C30B) were fabricated by a solution-casting method to study the effects of the clay loading on the crystallization behavior, thermal stability, and dynamic mechanical properties of PBAT in PBAT/C30B nanocomposites. X-ray diffraction and transmission electron microscopy results indicated the formation of exfoliated nanocomposites at low clay loadings (<5 wt %) and a mixture of exfoliated and intercalated nanocomposites with a clay content of 8 wt % throughout the PBAT matrix. Nonisothermal melt crystallization studies indicated that C30B enhanced the crystallization of PBAT, apparently because of a heterogeneous nucleation effect. Moreover, an attempt was made to quantitatively study the influence of the presence of C30B and its contents on the nucleation activity of PBAT in the PBAT/C30B nanocomposites. The thermal stability of PBAT decreased slightly in the nanocomposites. However, the storage modulus of PBAT apparently increased with the C30B loading increasing in the PBAT/C30B nanocomposites. © 2010 Wiley Periodicals, Inc. J Appl Polym Sci 119: 1426–1434, 2011

Key words: biodegradable; crystallization; nanocomposites

INTRODUCTION

Biodegradable polyesters have been widely studied in the last 2 decades. Among them, poly(butylene adipate-*co*-terephthalate) (PBAT), a commercially available, biodegradable, aliphatic–aromatic copolyester, is a flexible plastic designed for film extrusion and extrusion coating and is marketed by BASF (Tokyo, Japan) under the trademark Ecoflex. It can be synthesized by a polycondensation reaction of 1,4-butanediol with both adipic and terephthalic acids. The aromatic acid balances the mechanical reinforcement and biodegradability of the copolyester chains. The biodegradation behavior and properties of PBAT were studied by Müller and coworkers.[1–6] An aliphatic–aromatic copolyester with an aromatic unit concentration within the range of 35–55 mol % offers an optimal balance of biodegradability and physical properties. The crystal structure of PBAT has also been studied.[7–9] Kuwabara et al.[7] reported that a melt-crystallized PBAT sample contained small crystals with a wide size distribution; the crystalline region of PBAT is composed of butylene terephthalate (BT) units, whereas all butylene adipate (BA) units exist in a noncrystalline region. Cranston et al.[8] proposed a cocrystallization model for PBAT; that is, the BA portion adjusts its conformation to fit the crystal structure of poly(butylene terephthalate) because the adipic acid segments and terephthalic acid segments are similar in length. Kikutani and coworkers[9] found mixed crystallization of BT and BA monomers with solid ^{13}C-NMR and wide-angle X-ray diffraction (WAXD).

However, the use of these biodegradable thermoplastic copolyesters as general materials has still been restricted by their relatively high cost and poor mechanical properties. Blending with other polymers is an effective and simple way of modifying the properties of PBAT. The miscibility, thermal characterization, crystallization, and physical properties of poly(L-lactide) (PLLA)/PBAT blends have been investigated.[10–12] With increasing PBAT content

Correspondence to: Z. Qiu (qiuzb@mail.buct.edu.cn).

Contract grant sponsor: National Natural Science Foundation of China; contract grant numbers: 20974012, 20774013.

Contract grant sponsor: Program for New Century Excellent Talents in University; contract grant number: NCET-06-0101.

Contract grant sponsor: Program for Changjiang Scholars and Innovative Research Team in University; contract grant number: IRT0706.

Contract grant sponsor: Project of Polymer Chemistry and Physics of the Beijing Municipal Commission of Education; contract grant number: XK100100640.

(5–20 wt %), PLLA/PBAT blends showed decreased tensile strength and modulus; however, the elongation and toughness were dramatically increased. Strengthening of PBAT by melt blending with a liquid-crystalline polymer was also reported.[13] The tensile modulus of the blends increased gradually as the liquid-crystalline polymer content increased, and this indicated the excellent strengthening effects of the liquid-crystalline polymer on the PBAT matrix.

Another method for modifying biodegradable polymers is the combination of biodegradable polymers with cheap inorganic fillers or organic fillers, which not only provides a useful way of reducing the overall material cost but also enhances the mechanical properties (particularly the stiffness) while preserving acceptable ductility.[14–34] The microstructure, physical properties, and biodegradation of PBAT/organomodified montmorillonite nanocomposites were studied by Shibata and coworkers.[14,15] A PBAT/octadecylamine modified clay composite with a 5 wt % clay content showed the highest tensile modulus, strength, and elongation at break. The nonisothermal crystallization behavior of layered silicate microbiocomposites and nanobiocomposites based on PBAT was investigated with different theoretical models, which showed that the addition of a small amount of montmorillonite enhanced the nucleation of PBAT but also hindered the crystallite growth of PBAT in the composites.[16] Usually, the dispersion of clay particles in a polymer matrix results in the formation of two types of composite materials. First, there are intercalated polymer/clay nanocomposites, which are formed by the insertion of one or more polymer chains into the interlayer or gallery space of clays. Second, there are exfoliated or delaminated polymer/clay nanocomposites, which are formed when clay nanolayers are individually dispersed in a continuous polymer matrix. An enhancement of the physical properties and crystallization behavior can often be achieved with very low clay loadings.

In general, it is believed that property improvements in polymer/clay nanocomposites, in comparison with conventional composites, come from interfacial interactions between the polymer matrix and organically modified layered silicate.[35,36] Cloisite 30B (C30B) is a commercially available organoclay. According to the supplier, the original clay montmorillonite was modified with 30 wt % methyl tallow quaternary ammonium salt.[37] In this work, biodegradable PBAT/C30B nanocomposites were prepared because both are commercially available; furthermore, much more attention has been paid to the effect of C30B on the nonisothermal melt crystallization and thermal and dynamic properties of PBAT in PBAT/C30B nanocomposites.

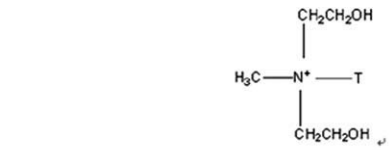

Where T is Tallow (~65% C18; ~30% C16; ~5% C14)

Anion: Chloride

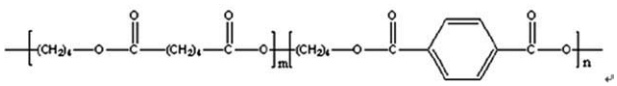

Scheme 1 Chemical structures of C30B and PBAT.

EXPERIMENTAL

Materials

PBAT (weight-average molecular weight = 6.23×10^4, number-average molecular weight = 3.82×10^4, weight-average molecular weight/number-average molecular weight = 1.63) was kindly supplied by BASF. It is a copolymer with a BT content of 44 mol %. C30B was purchased from Southern Clay Products (Gonzales, TX); it contains methyl-bis(2-hydroxyethyl) tallow alkyl ammonium cations. The chemical structures of PBAT and C30B are shown in Scheme 1 (T denotes tallow, which is ~ 65% C18, ~ 30% C16, and ~ 5% C14).

Preparation of the PBAT/C30B nanocomposites

C30B and PBAT were dried *in vacuo* at 50°C for at least 24 h before use. PBAT/C30B nanocomposites were prepared with the solution-intercalation-casting technique. Clay dispersions (<0.1 wt %) were obtained by the suspension of dried clay in a separate beaker of chloroform. The clay suspension was sonicated for 1 h with a KQ3200E probe sonicator (Ultrasonic Instrument Co., Ltd., in Kunshan City, Jiangsu, China) at a power of 150 W at room temperature. At the same time, PBAT was dissolved in the proper amount of chloroform (1 g/10 mL) at room temperature. Then, the clay suspension and the PBAT solution were mixed together. The obtained mixture was further sonicated and stirred for 6 h. The mixture was cast onto a glass surface and kept *in vacuo* at 50°C for 3 days to remove the solvent completely. PBAT was mixed with various amounts of C30B (2, 5, and 8 wt %) in the polymer matrix. For brevity, the nanocomposites with 2, 5, and 8 wt % C30B are abbreviated as C30B-2, C30B-5, and C30B-8, respectively.

Characterization

WAXD patterns were recorded with a Rigaku D/Max 2500 VB2t/PC X-ray diffractometer (Tokyo, Japan). The Cu Kα radiation source (wavelength = 0.154 nm) was operated at 40 kV and 200 mA. The

samples were first pressed into films with a thickness of approximately 0.5 mm on a hot stage at 170°C and then transferred into a vacuum oven at 90°C for 58 h. WAXD patterns were recorded from 0 to 10° at 1°/min and from 5 to 50° at 4°/min.

Transmission electron microscopy (TEM) was employed to observe the dispersion of C30B in the nanocomposites. TEM observation of the PBAT/C30B nanocomposites was performed with a Hitachi H-800 TEM instrument (Tokyo, Japan) under an acceleration voltage of 200 kV. Thin sections (ca. 50–70 nm thick) for TEM observations were cut from the as-prepared nanocomposites under cryogenic conditions (−80°C) with a Leica EM FC6 ultramicrotome.

Thermal analysis was carried out with a TA Instruments Q100 differential scanning calorimeter with Universal Analysis 2000 (New Castle, Delaware). All operations were performed under a nitrogen purge, and the weight of the samples varied from 5 to 5.5 mg. Nonisothermal melt crystallization was employed to study the crystallization behavior of neat PBAT and its nanocomposites. The samples were first heated to 170°C at 40°C/min, held at 170°C for 3 min to erase any thermal history, and cooled to 20°C at different constant cooling rates ranging from 2 to 10°C/min. The crystallization peak temperature (T_p) was obtained from the cooling traces. The samples were heated to 170°C again at 20°C/min to study the subsequent melting behavior.

The spherulitic morphology of neat PBAT and the PBAT/C30B nanocomposites was observed under an Olympus BX51 polarizing microscope with a temperature controller (THMS 600, Linkam, Surrey, England). The samples were first annealed at 170°C for 3 min to erase any thermal history and then cooled to 120°C at 40°C/min.

A Q50 thermogravimetric analyzer from TA Instruments was used to determine the degradation temperatures of pure PBAT, pure C30B, and the PBAT/C30B nanocomposites. The sample was heated to 580°C at a heating rate of 20°C/min. Nitrogen was used as the purge gas with the sample purge being 60 mL/min.

Dynamic mechanical analysis (DMA) was performed on samples (42 mm × 7 mm × 0.2 mm) with a Netzsch 242 dynamic mechanical analyzer (Bavarian town of Selb, Germany) under the tension film mode in the temperature range of −100 to 60°C at a frequency of 1 Hz with a strain amplitude of 0.02% and a heating rate of 5°C/min.

RESULTS AND DISCUSSION

Morphology of the PBAT/C30B nanocomposites by WAXD and TEM

The dispersion of clay in the PBAT/C30B nanocomposites was investigated with WAXD and TEM.

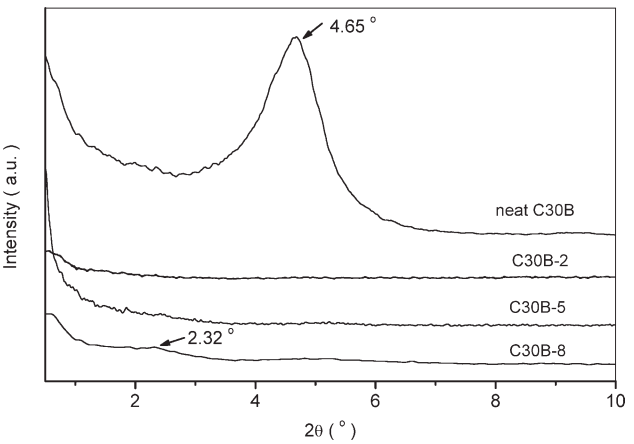

Figure 1 WAXD patterns of neat C30B and the PBAT/C30B nanocomposites.

Figure 1 shows the WAXD patterns of neat C30B and the PBAT/C30 nanocomposites with different clay loadings. The WAXD pattern of pure C30B shows a diffraction peak at approximately $2\theta = 4.65°$, which corresponds to a basal spacing of 19.0 Å. After its incorporation with PBAT, the diffraction peak of C30B disappeared in the WAXD patterns for the PBAT/C30B nanocomposites with clay loadings lower than 5 wt %. The absence of the diffraction peak indicates the formation of an exfoliated structure.

Despite the absence of the diffraction peak, a broad shoulder in the small-angle region can be observed in the WAXD pattern for the PBAT/C30B nanocomposite with a clay loading up to 8 wt %; this probably indicates the formation of an intercalated structure. Figure 1 shows a diffraction peak at about $2\theta = 2.32°$ for the C30B-8 nanocomposite, which corresponds to a basal spacing of 38.0 Å.

The PBAT/C30B nanocomposites were further detected by TEM. As shown in Figure 2, the TEM images show typical but different clay dispersions for samples C30B-5 and C30B-8. Exfoliated nanocomposites were obtained when the organoclay content was lower than 5 wt %, as shown in Figure 2(a). The clay platelets (separate dark lines) were well dispersed in the PBAT matrix. For C30B-8, intercalated/exfoliated structures coexisted, as shown in Figure 2(b).

It is thought that the relative fraction of intercalation and exfoliation usually increases with an increasing organoclay concentration. This is illustrated by a smooth shoulder in the diffraction intensity at a low angle in the WAXD pattern, which probably suggests a complex structure. At a high clay loading (e.g., C30B-8), clay agglomeration is usually inevitable to some extent. In addition, diverse nanoscale morphologies of clay are usually

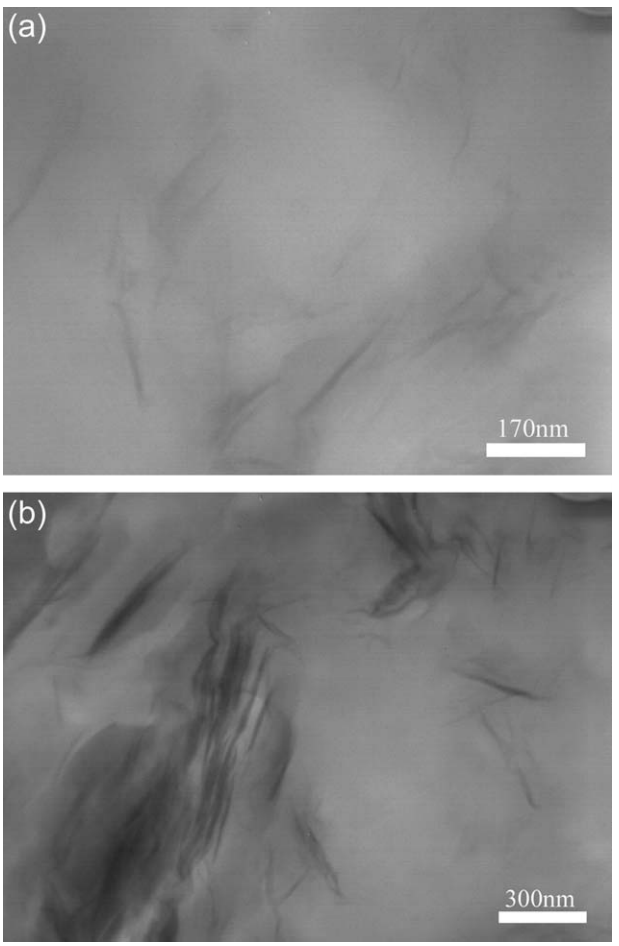

Figure 2 TEM images of PBAT/C30B nanocomposites: (a) C30B-5 and (b) C30B-8.

observed by TEM. Similar results were observed by Liu et al.[38] for nylon 11/clay nanocomposites.

Crystallization of neat PBAT and the PBAT/C30B nanocomposites

Basic thermal properties are very important for the study of the crystallization behavior of polymeric materials. In this work, the glass-transition temperature (T_g) of PBAT remained almost unchanged despite the addition of C30B, whereas the melting temperature (T_m) increased slightly with the C30B loading increasing in the nanocomposites. The basic thermal properties remained almost unchanged and, therefore, did not play a dominant role in the crystallization behavior of neat PBAT and its nanocomposites with different clay loadings.

An understanding of polymer crystallization behavior under dynamic conditions is also of great importance for optimizing the processing conditions to obtain desired product properties because most processing techniques actually occur under nonisothermal conditions. The nonisothermal melt crystallization of neat PBAT and the PBAT/C30B nanocomposites was studied with differential scanning calorimetry (DSC) at different cooling rates in this work.

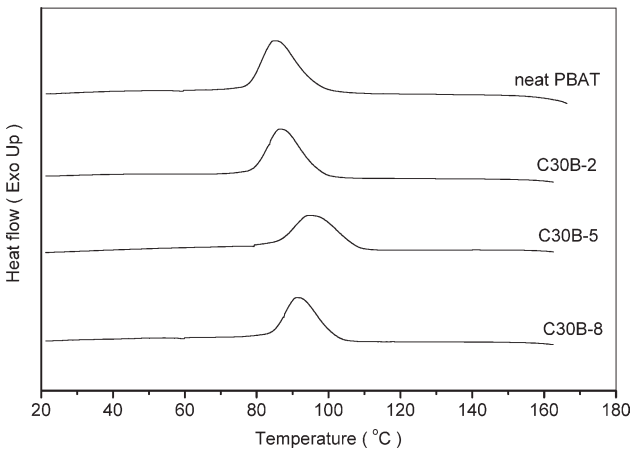

Figure 3 DSC cooling traces of neat PBAT and the PBAT/C30B nanocomposites at 10°C/min.

Figure 3 shows DSC cooling traces of neat PBAT and its three nanocomposites from the melt at 10°C/min as examples. T_p was approximately 80.3°C for neat PBAT and shifted to a high temperature range in the presence of C30B. For C30B-2, T_p shifted to approximately 86.8°C. With the C30B loading further increasing, T_p shifted to approximately 94.8°C for C30B-5; however, T_p was approximately 91.5°C for C30B-8. These results indicated that the presence of C30B enhanced the crystallization of PBAT in the PBAT/C30B nanocomposites; moreover, the enhancement was affected significantly by the C30B contents. In brief, T_p of PBAT shifted to high temperatures in the presence of C30B; furthermore, this increase in T_p was significant when the C30B concentration was less than 5 wt %.

To show the effects of the cooling rates and the C30B contents on nonisothermal melt crystallization, Figure 4 summarizes the variation of T_p with the

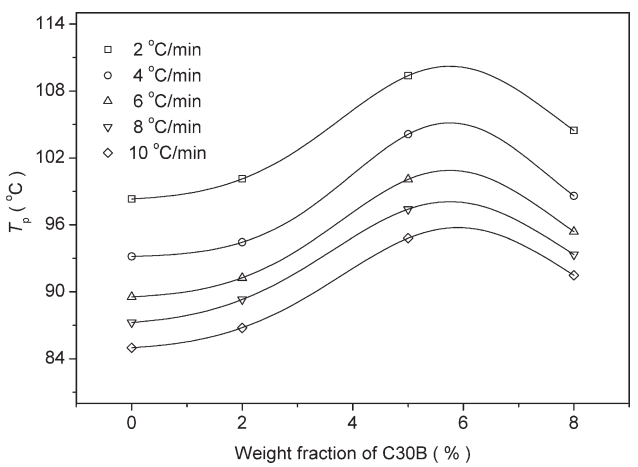

Figure 4 Effect of the C30B loadings on T_p for neat PBAT and the PBAT/C30B nanocomposites at different cooling rates.

cooling rate for neat PBAT and its three nanocomposites. The effects of the cooling rates and the C30B contents on the variation of T_p were determined. Figure 4 shows that the T_p values of PBAT in the nanocomposites were higher than T_p of neat PBAT at a given cooling rate; moreover, T_p shifted to a high temperature range with an increasing C30B concentration in the PBAT/C30B nanocomposites when the C30B concentration was lower than 5 wt %. These results indicated again that the nonisothermal melt crystallization of PBAT was enhanced by the presence of C30B, and the degree of enhancement of T_p was apparently influenced by the clay loading. From the aforementioned studies, it is clear that the presence of C30B and its concentration have a significant effect on the nonisothermal melt crystallization behavior of PBAT because of the heterogeneous nucleation agent effect. In addition, the T_p values of neat PBAT and the nanocomposites decreased with increasing cooling rates because the samples did not have enough time to crystallize in the high temperature range at higher cooling rates.

Ozawa[39] extended the Avrami equation for isothermal crystallization to the nonisothermal case by assuming that a sample is cooled at a constant rate from the molten state. In the Ozawa method, the time variable in the Avrami equation is replaced by a cooling rate (Φ), and the relative crystallinity (X_t) is derived as a function of constant Φ:

$$X_t = 1 - \exp[-K(T)/\Phi^m] \quad (1)$$

where $K(T)$ is the cooling (or heating) function at crystallization temperature T, which is related to both nucleation and crystal growth, and m is the Ozawa exponent, which depends on the type of nucleation and growth mechanism.[40–42] Double logarithms of eq. (1) and rearrangement resulted in the following form:

$$\log[-\ln(1 - X_t)] = \log K(T) - m \log \Phi \quad (2)$$

Figure 5 shows Ozawa plots for neat PBAT and the C30B-2 and C30B-5 nanocomposites. As shown in Figure 5(a,b), a series of straight lines were obtained. Therefore, it can be concluded that the Ozawa method can describe the nonisothermal crystallization process successfully within the studied crystallization temperature range for neat PBAT and the C30B-2 nanocomposite. However, it is obvious from Figure 5(c) that the Ozawa equation fails to describe the nonisothermal crystallization process of the C30B-5 nanocomposite. Similarly, the Ozawa equation also fails to fit the nonisothermal melt crystallization of the C30B-8 sample. The failure of the Ozawa equation to fit the nonisothermal melt crystallization of the PBAT/C30B nanocomposites probably arises from the secondary crystallization of PBAT in the further presence of C30B in the PBAT/C30B nanocomposites because Ozawa took no account of the secondary crystallization. Secondary crystallization may arise from any of the following processes: crystallization of shorter or less perfect chains of the principal polymers, crystallization of intentionally or unintentionally added chains of other species, crystallization of the principal polymer

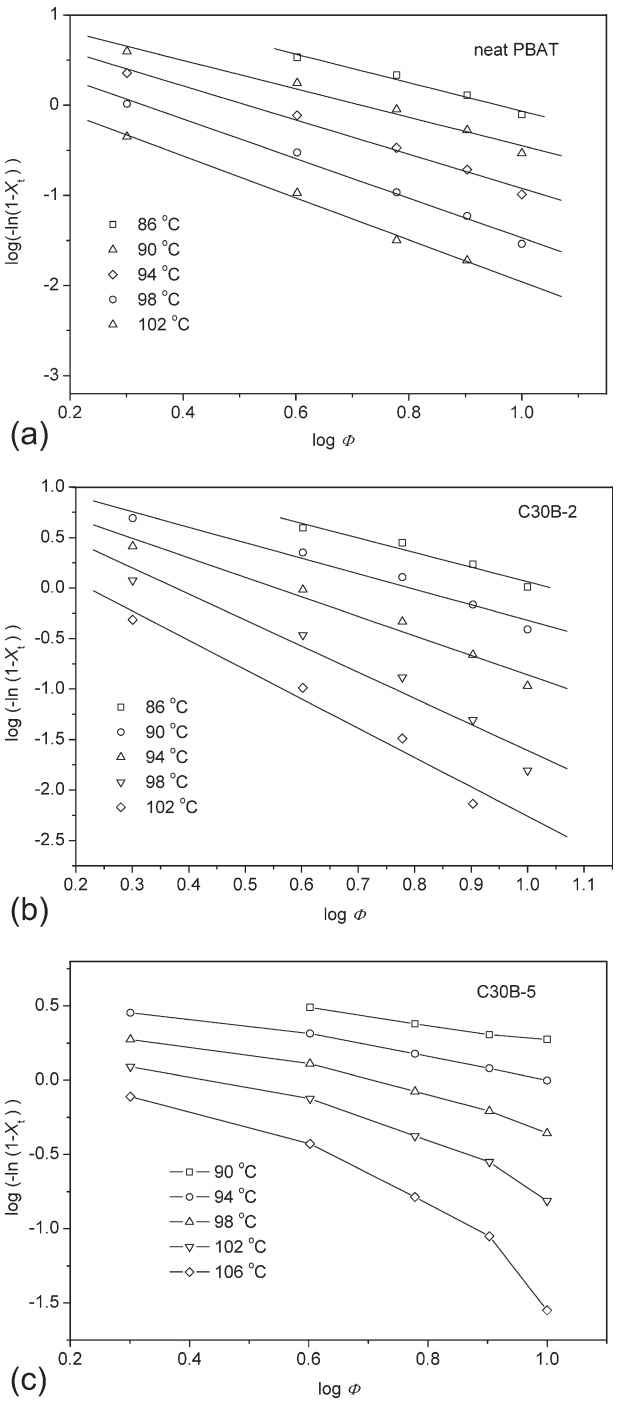

Figure 5 Ozawa plots of (a) neat PBAT, (b) the C30B-2 nanocomposite, and (c) the C30B-5 nanocomposite.

TABLE I
Parameters of the Nonisothermal Melt Crystallization Kinetics of Neat PBAT and the C30B-2 Nanocomposite Based on the Ozawa Equation

Sample	T (°C)	$K(T)^m$ (°C/min)	m
Neat PBAT	86	44.10	2.0
	90	31.89	2.0
	94	10.79	2.0
	98	6.74	2.4
	102	2.51	2.4
C30B-2	86	112.76	2.0
	90	41.81	2.0
	94	13.20	2.0
	98	6.88	2.3
	102	3.00	2.5

in small volume packets remaining after the primary transformation phase, further growth of crystals formed during primary crystallization, and increasing perfection of crystals formed during primary crystallization.[43] It is generally believed that the secondary crystallization of PBAT/C30B nanocomposites with different C30B loadings is caused by the increasing perfection of crystals formed during primary crystallization.[44]

As shown in Table I, the values of m were between 2.0 and 2.5 for neat PBAT and a C30B-2 nanocomposite in the detected temperature range, and this indicates that the crystallization may correspond to three-dimensional truncated spherulitic growth with athermal nucleation for neat PBAT and the C30B-2 nanocomposite.[45] The values of m were approximately 2.0 at a crystallization temperature not higher than 94°C and approximately 2.4 at a temperature higher than 98°C for both neat PBAT and the C30B-2 nanocomposite. The results indicate that the crystallization mechanism may have changed at temperatures below and above 98°C. However, the exact reasons are still uncertain and need further investigation. The fact that m does not apparently change with the addition of C30B at the same temperature also indicates that the crystallization mechanism does not change. The values of $K(T)$ are also shown in Table I. The values of $K(T)$ decreased with increasing crystallization temperature within the temperature range investigated for both neat PBAT and the C30B-2 nanocomposite, and this suggests that crystallization was retarded at a higher temperature. Moreover, $K(T)$ increased with the addition of C30B at the same temperature, and this suggests that the crystallization was accelerated by the addition of C30B.

From the aforementioned studies, it is obvious that the nonisothermal melt crystallization of PBAT was enhanced by the presence of C30B in the PBAT/C30B nanocomposites because of the heterogeneous nucleation effect. In this section, the effects of C30B and its contents on the nucleation activity of PBAT in the PBAT/C30B nanocomposites are evaluated quantitatively.

The nucleation activity of a foreign substrate with respect to the crystallization of a polymer can be estimated with a method developed by Dobreva and Gutzow.[46,47] For homogeneous nucleation from the melt, Φ can be written as follows:

$$\log \Phi = A - B/2.303\Delta T_p^2 \tag{3}$$

where ΔT_p is defined as $T_m - T_p$ and A and B are constants. For heterogeneous nucleation, Φ is defined as follows:

$$\log \Phi = A' - B^*/2.303\Delta T_p^2 \tag{4}$$

where A' and B^* are constants. The B^*/B ratio is defined as the nucleating activity. If the foreign substrate is extremely active, the nucleating activity approaches 0, whereas for inert particles, it approaches 1.

Figure 6 shows plots of log Φ against $1/\Delta T_p^2$; the values of B for neat PBAT and the values of B^* for its three nanocomposites with different C30B contents were obtained from the slopes. Thus, the values of the nucleating activity were determined to be 0.73, 0.34, and 0.68 for the C30B-2, C30B-5, and C30B-8 nanocomposites, respectively. All the nucleating activity values were less than 1, and this indicated that C30B acted as a nucleating agent for the crystallization of PBAT. Moreover, the nucleation activity was first improved with increasing C30B contents when the clay loadings were lower than 5 wt % and then decreased when the C30B loading further increased to 8 wt %. The results were attributed to clay agglomeration at high clay loadings (e.g.,

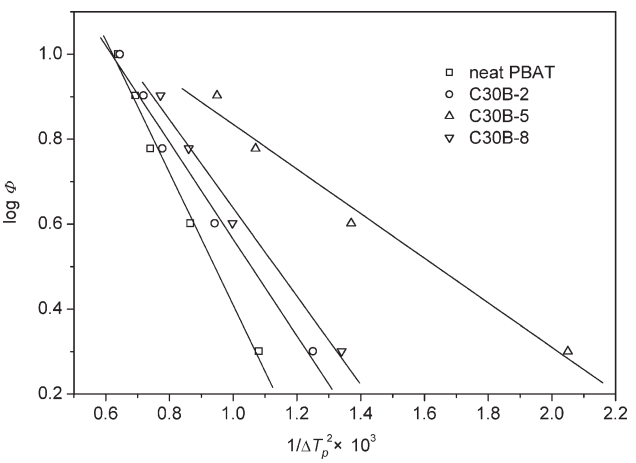

Figure 6 Plots of log Φ versus $1/\Delta T_p^2$ for the estimation of the nucleation activity of the PBAT/C30B nanocomposites with different C30B loadings.

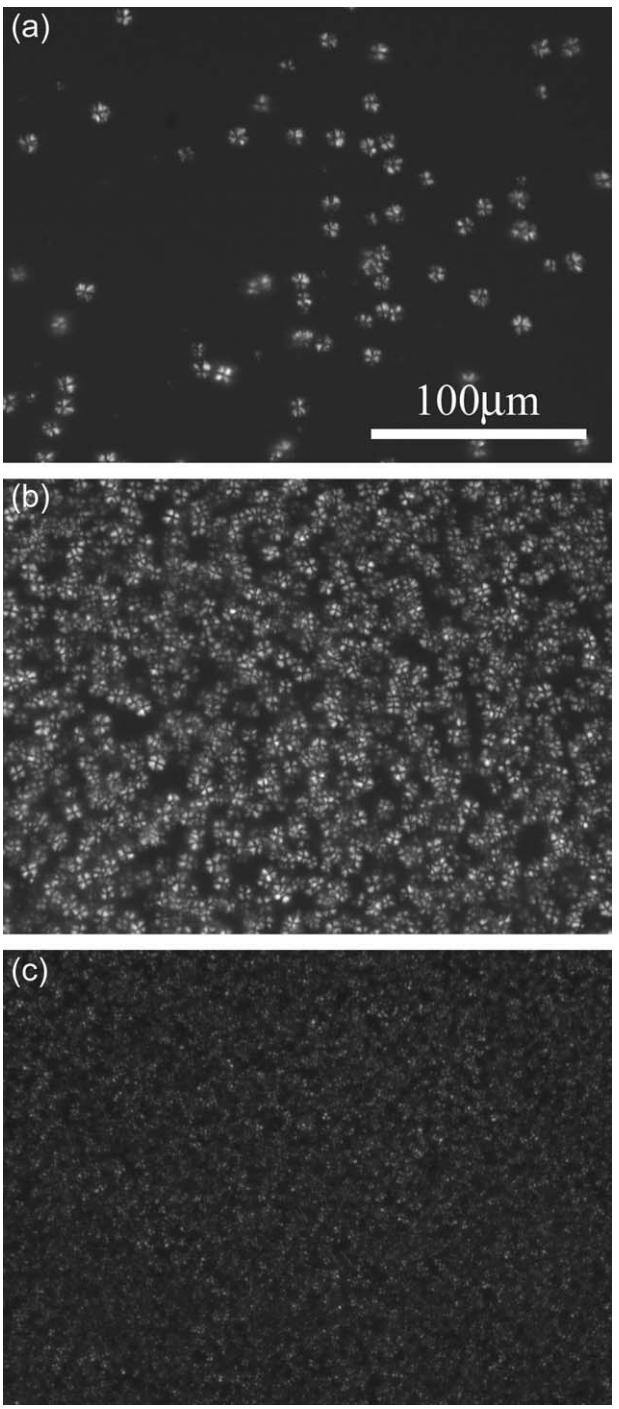

Figure 7 POM images of (a) neat PBAT, (b) the C30B-2 nanocomposite, and (c) the C30B-5 nanocomposite crystallized at 120°C for 30 min from the melt.

C30B-8), which decreased the nucleation effect of C30B.

The spherulitic morphology of neat PBAT and its nanocomposites was further studied with polarized optical microscopy (POM). Figure 7 illustrates the spherulitic morphology of neat PBAT and a C30B-2 sample crystallized at 120°C for 30 min. Figure 7(a) shows that the well developed spherulites grew to a diameter of roughly 7–8 μm with a relatively low density for neat PBAT. However, Figure 7(b,c) shows that the PBAT spherulites became smaller and the density increased significantly with an increase in C30B; this was indicative of a heterogeneous nucleation effect of C30B. It is obvious that the nucleation density of the PBAT spherulites increased in the presence of C30B in the PBAT/C30B nanocomposites because of their nucleation agent effect. In conclusion, the presence of C30B and its contents in the PBAT matrix had a significant influence on the spherulitic morphology and overall crystallization process of PBAT.

The crystal structure of PBAT before and after nanocomposite preparation with C30B was investigated with WAXD. Figure 8 shows the WAXD patterns of neat PBAT and the PBAT/C30B nanocomposites crystallized at 90°C for 58 h. Neat PBAT and its nanocomposites with different clay loadings exhibited almost the same diffraction peaks at almost the same locations, and this indicated that the incorporation of C30B did not modify the crystal structure of PBAT.

Thermal stability and dynamic mechanical properties of neat PBAT and the PBAT/C30B nanocomposites

The thermal stability of pure PBAT, pure C30B, and the PBAT/C30B nanocomposites were investigated by thermogravimetric analysis (TGA) under nitrogen. Figure 9(a,b) displays the TGA and first derivative thermogravimetry (DTG) curves of neat PBAT, neat C30B, and the PBAT/C30B nanocomposites, respectively. As shown in Figure 9(a), the decomposition temperature at a 5 wt % weight loss (T_d) decreased with the clay loading increasing. For neat PBAT, T_d was approximately 377.9°C. However, T_d was only 263.8°C for neat C30B because of the

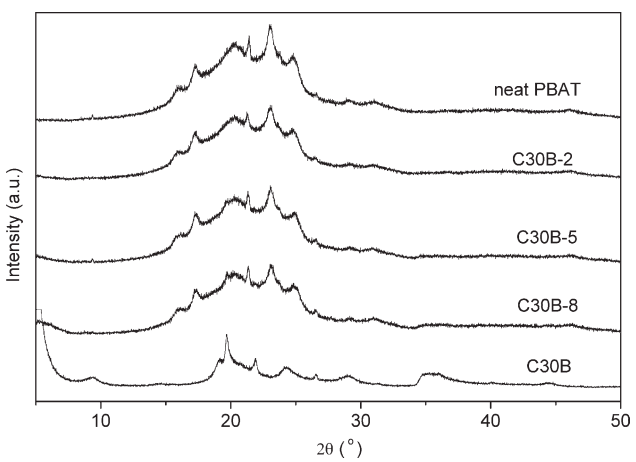

Figure 8 WAXD patterns of neat PBAT and the PBAT/C30B nanocomposites crystallized at 90°C for 58 h.

organic groups, as shown in Scheme 1. For the PBAT/C30B nanocomposites, T_d shifted to approximately 378.7, 372.7, and 368.3°C with the C30B loading increasing from 2 to 8 wt % in the PBAT/C30B nanocomposites. It is obvious that the thermal stability of the PBAT/C30B nanocomposites decreased slightly versus that of neat PBAT because of the presence of C30B with lower thermal stability.

The temperature of the maximal decomposition rate (T_{max}) was obtained from the DTG curves, as shown in Figure 9(b). T_{max} was 419.4°C for neat PBAT and became 422.2, 417.9, and 418.8°C for the C30B-2, C30B-5, and C30B-8 samples, respectively. It is obvious that the presence of C30B and its loadings did not influence the T_{max} values of the PBAT/C30B nanocomposites significantly.

DMA was performed to study the influence of the C30B loading on the storage modulus (E') of PBAT in the PBAT/C30B nanocomposites. Figure 10 summarizes the E' data in the temperature range of −90 to 60°C. As shown in Figure 10, there was a significant enhancement of E' for all the PBAT/C30B nanocomposites when the temperature was below T_g. For example, the increments in E' were approximately 40% for the C30B-2 sample, 46% for the C30B-5 sample, and 55% for the C30B-8 sample at −50°C versus

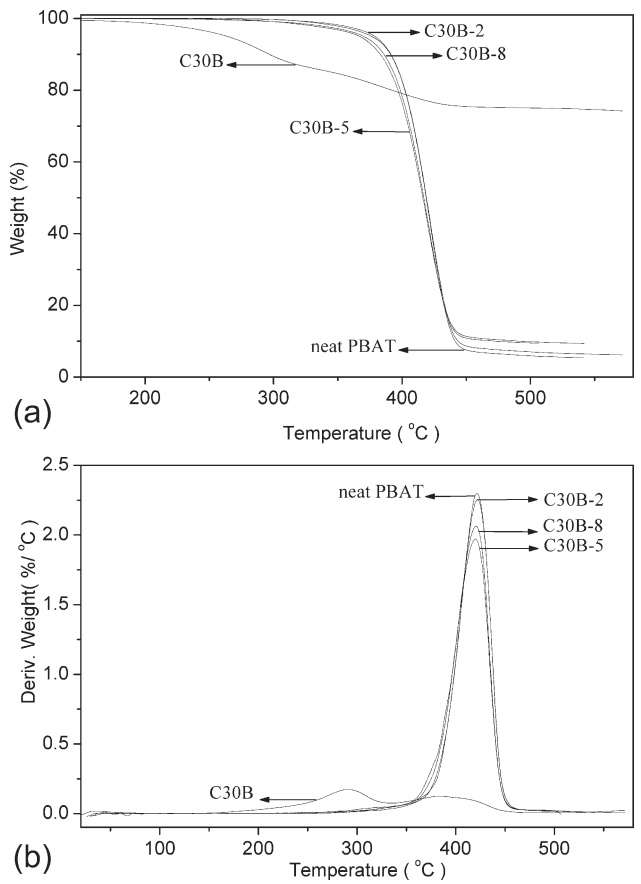

Figure 9 (a) TGA and (b) DTG curves of neat PBAT and the PBAT/C30B nanocomposites.

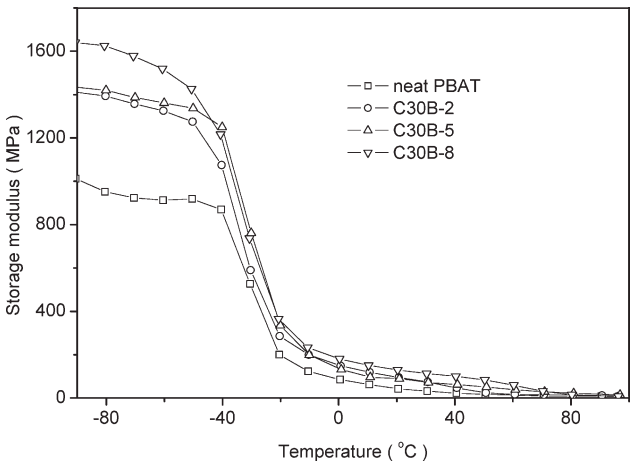

Figure 10 Temperature dependence of E' for neat PBAT and the PBAT/C30B nanocomposites.

that of neat PBAT. However, the degree of enhancement of E' showed a different temperature dependence for the PBAT/C30B nanocomposites. At −30°C, E' was enhanced to 577.1 MPa for the C30B-2 nanocomposite from 514.1 MPa for neat PBAT, and this was indicative of an increase of approximately 12%. At 0°C, E' increased to approximately 151.6 MPa for the C30B-2 nanocomposite from approximately 83.8 MPa for neat PBAT, and this was indicative of an increase of approximately 81%. Furthermore, E' improved to approximately 47.1 MPa for the C30B-2 nanocomposite from approximately 23.1 MPa for neat PBAT at 40°C, and this was indicative of an increase of approximately 104%. The C30B-5 and C30B-8 nanocomposites showed a temperature dependence of the enhancement of E' similar to that of the C30B-2 nanocomposite.

CONCLUSIONS

Intercalated and exfoliated nanocomposites of biodegradable PBAT and C30B were fabricated by a solution-casting method to study the effect of the clay loading on the crystallization behavior and physical properties of PBAT in PBAT/C30B nanocomposites. The exfoliated nanocomposites were obtained at low clay concentrations (<5 wt %), whereas a mixture of exfoliated and intercalated nanocomposites was prepared with a clay content of 8 wt % throughout the PBAT matrix. Nonisothermal melt crystallization studies suggested that C30B enhanced the crystallization of PBAT, apparently because of a heterogeneous nucleation effect. The Ozawa method was found to be appropriate for describing the nonisothermal crystallization process of neat PBAT and the C30B-2 nanocomposite but failed to describe the process for the C30B-5 and C30B-8 nanocomposites; this was ascribed to the secondary crystallization of PBAT by the adequate addition of C30B. Moreover, an

attempt was made to study the effect of the presence of C30B and its contents on the nucleation activity of PBAT in the PBAT/C30B nanocomposites quantitatively. As a result, the C30B-5 nanocomposite was found to have the maximum nucleation activity. The thermal stability of the PBAT/C30B nanocomposites decreased slightly versus that of neat PBAT because of the presence of C30B with lower thermal stability. DMA results showed that E' of the PBAT/C30B nanocomposites apparently increased with respect to that of neat PBAT.

The authors thank BASF for kindly providing the PBAT samples.

References

1. Witt, U.; Einig, T.; Yamamoto, M.; Kleeberg, I.; Deckwe, W.; Müller, R. Chemosphere 2001, 44, 289.
2. Kijchavengkul, T.; Auras, R.; Rubino, M.; Ngouajio, M.; Fernandez, R. Chemosphere 2008, 71, 1607.
3. Witt, U.; Müller, R.; Deckwer, W. Macromol Chem Phys 1996, 197, 1525.
4. Witt, U.; Müller, R.; Deckwer, W. J Environ Polym Degrad 1995, 3, 215.
5. Witt, U.; Müller, R.; Deckwer, W. J Environ Polym Degrad 1997, 5, 81.
6. Rantze, E.; Kleeberg, I.; Witt, U.; Müller, R.; Deckwer, W. Macromol Symp 1998, 130, 319.
7. Kuwabara, K.; Gan, Z.; Nakamura, T.; Abe, H.; Doi, Y. Biomacromolecules 2002, 3, 390.
8. Cranston, E.; Kawada, J.; Raymond, S.; Morin, F.; Marchessault, R. Biomacromolecules 2003, 4, 995.
9. Shi, X.; Ito, H.; Kikutani, T. Polymer 2005, 46, 11442.
10. Liu, T.; Lin, W.; Yang, M.; Chen, S. Polymer 2005, 46, 12586.
11. Jiang, L.; Wolcott, M.; Zhang, J. Biomacromolecules 2006, 7, 199.
12. Coltelli, M.; Maggiore, I.; Bertoldo, M.; Signori, F.; Bronco, S.; Ciardelli, F. J Appl Polym Sci 2008, 110, 1250.
13. Iwakura, Y.; Li, Y.; Nakayama, K.; Shimizu, H. J Appl Polym Sci 2008, 109, 333.
14. Someya, Y.; Sugahara, Y.; Shibata, M. J Appl Polym Sci 2005, 95, 386.
15. Someya, Y.; Kondo, N.; Shibata, M. J Appl Polym Sci 2007, 106, 730.
16. Chivrac, F.; Pollet, E.; Avérous, L. J Polym Sci Part B: Polym Phys 2007, 45, 1503.
17. Nakane, K.; Yamashita, T.; Iwakura, K.; Suzuki, F. J Appl Polym Sci 1999, 74, 133.
18. Chang, J.; Jang, T.; Ihn, K.; Lee, W.; Sur, G. J Appl Polym Sci 2003, 90, 3208.
19. Ray, S.; Maiti, P.; Okamoto, M.; Yamada, K.; Ueda, K. Macromolecules 2002, 35, 3104.
20. Krikorian, V.; Pochan, D. Chem Mater 2003, 15, 4317.
21. Krikorian, V.; Pochan, D. Macromolecules 2004, 37, 6480.
22. Pluta, M.; Jeszka, J.; Boiteux, G. Eur Polym J 2007, 43, 2819.
23. Lyu, S.; Park, D.; Bae, K.; Sur, G. Polym Korea 2001, 25, 421.
24. Chrissafis, K.; Antoniadis, G.; Paraskevopoulos, K.; Vassiliou, A.; Bikiaris, D. Compos Sci Technol 2007, 67, 2165.
25. Ray, S.; Okamoto, K.; Maiti, P.; Okamoto, M. J Nanosci Nanotech 2002, 2, 1.
26. Ray, S.; Okamoto, K.; Okamoto, M. Macromolecules 2003, 36, 2355.
27. Someya, Y.; Nakazato, T.; Teramoto, N.; Shibata, M. J Appl Polym Sci 2004, 91, 1463.
28. Shih, Y.; Wang, T.; Jeng, R.; Wu, J.; Teng, C. J Polym Environ 2007, 15, 151.
29. Chen, G.; Yoon, J. J Polym Sci Part B: Polym Phys 2005, 43, 817.
30. Ray, S.; Bousmina, M.; Okamoto, K. Macromol Mater Eng 2005, 290, 759.
31. Ray, S.; Bandyopadhyay, J.; Bousmina, M. Polym Degrad Stab 2007, 92, 802.
32. Ray, S.; Bousmina, M. Macromol Chem Phys 2006, 207, 1207.
33. Maiti, P.; Carl, A. B.; Giannelis, E. Biomacromolecules 2007, 8, 3393.
34. Wang, S.; Song, C.; Chen, G.; Guo, T.; Liu, J.; Zhang, B.; Takeuchic, S. Polym Degrad Stab 2005, 87, 69.
35. Ray, S.; Okamoto, M. Prog Polym Sci 2003, 28, 1539.
36. Ray, S.; Bousmina, M. Polymer 2005, 46, 12430.
37. Cloisite 30B Data Sheet; Southern Clay Products: Gonzales, TX, 2010.
38. Liu, T.; Lim, K.; Tjiu, W.; Pramoda, K.; Chen, Z. Polymer 2003, 44, 3529.
39. Ozawa, T. Polymer 1971, 12, 150.
40. Qian, J.; Zhu, L.; Zhang, J.; Whitehouse, R. J Polym Sci Part B: Polym Phys 2007, 45, 1564.
41. Apiwanthanakorn, N.; Supaphol, P.; Nithitanakul, M. Polym Test 2004, 23, 817.
42. Qiu, Z.; Yang, W. J Appl Polym Sci 2007, 104, 972.
43. Schultz, J. Polymer Crystallization; Oxford University Press: Oxford, 2001; Chapter 9.
44. Xiao, H.; Lu, W.; Yeh, J. J Appl Polym Sci 2009, 112, 3754.
45. Wunderlich, B. Macromolecular Physics; Academic: New York, 1976; Vol. 2, Chapter 20, p 147.
46. Dobreva, A.; Gutzow, I. J Non-Cryst Solids 1993, 162, 1.
47. Dobreva, A.; Gutzow, I. J Non-Cryst Solids 1993, 162, 13.